ACS OMEGA

Open Access

This article is licensed under CC-BY-NC-ND 4.0

http://pubs.acs.org/journal/acsodf

Article

Polarization-Independent Perfect Absorption in Monolayer Black Phosphorus Metasurfaces at Terahertz Frequencies via Critical Coupling

Xuewen Long,* Jing Bai, Yingjun Zhang, Mingshan Zhu, Xiuli Guo, Jin Wang, Weiqiang Wang, and Rui Lou

Cite This: *ACS Omega* 2024, 9, 35052−35059

Read Online

ACCESS | Metrics & More | Article Recommendations

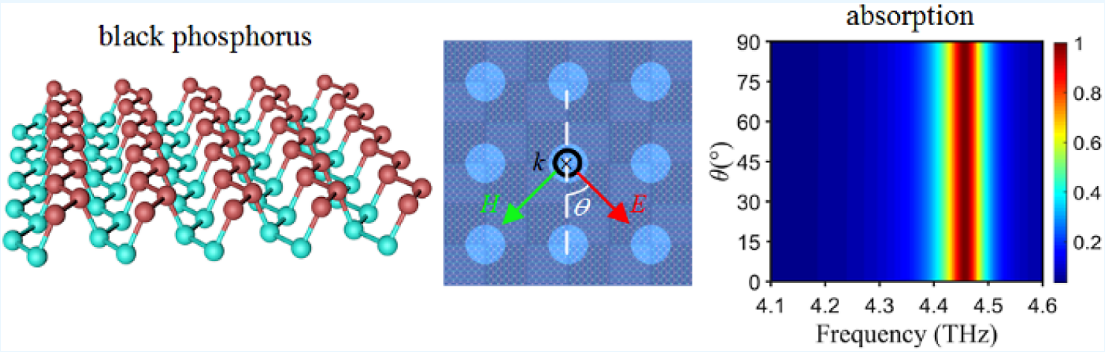

ABSTRACT: Two-dimensional (2D) materials, which possess rich underlying physical properties that can provide the potential for designing more efficient and compact optoelectronic devices, have attracted great interest among scientists. Due to the atomic-scale thickness and the anisotropy of in-plane conductivity, 2D black phosphorus (BP) exhibits a polarization-dependent absorption spectrum with low absorption, which limits its further development in polarization-independent applications such as light absorbers and sensors. In this paper, a polarization-independent perfect absorber in the terahertz band is proposed, which is composed of a patterned BP monolayer deposited on a lossless photonic crystal (PC) slab with a back reflection mirror. The absorption of the patterned BP monolayer can reach 100% at resonant frequencies through the critical coupling mechanism of guided resonance. Moreover, the absorber exhibits polarization-independent absorption characteristics for vertically incident light, which are attributed to the 4-fold rotational symmetry of the PC substrate and the patterned BP monolayer deposited on it. This work opens up the possibility of fabricating optically polarization-independent devices based on single-layer 2D anisotropic materials.

1. INTRODUCTION

Atomically thin 2D materials were proposed with the successful separation of graphene, a single atomic layer graphite material, by Geim's team at the University of Manchester in 2004.[1] 2D materials exhibit many unique electronic, optical, and thermal properties that traditional materials do not possess due to their carrier migration and heat diffusion being confined within the thin 2D plane, offering the possibility for constructing high-performance and new functional ultracompact electronic, photonic, and optoelectronic devices and attracting great interest from scientists in the past two decades. Considering the low intrinsic optical absorption efficiency owing to the ultrathin thickness of 2D materials, enhancing the interaction between light and 2D materials is of great significance for many high-efficiency devices, related applications, and fundamental research. So far, many mechanisms have been proposed to achieve optical absorption enhancement for 2D materials, including surface plasmon polaritons,[2] Tamm plasmon polaritons,[3] local plasmons,[4] Fano resonance,[5] Fabry−Perot resonance,[6−8] critical coupling,[9−18] etc.

As a newly emerged member of the 2D material family in recent years, BP shows much richer physics than other 2D materials, including exhibiting ultrahigh charge carrier mobility and a layer-dependent band gap ranging from 0.3 eV in bulk to 2 eV for the monolayer form, thus showing an excellent optical response from the visible to the infrared region, and this makes

Received: June 3, 2024
Revised: July 19, 2024
Accepted: July 26, 2024
Published: August 2, 2024

© 2024 The Authors. Published by American Chemical Society

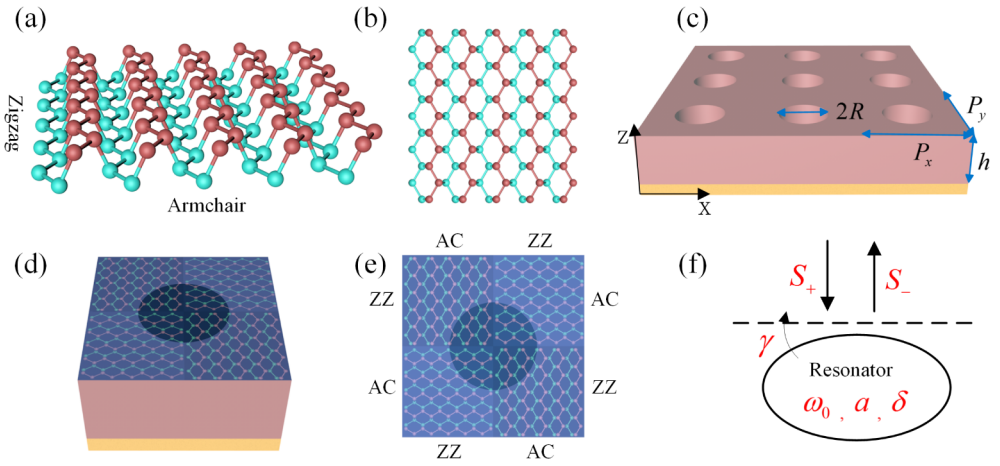

Figure 1. (a) Schematic of the monolayer BP. (b) Top view of the monolayer BP. (c) Schematic of a PC slab with circular air holes stacked on a metal reflector layer. Yellow represents the metal reflector layer. The thickness, periodicity of the PC slab, and the radius of the air holes are marked with the corresponding letters in the figure. (d) One unit of the proposed compound absorber with patterned BP. (e) Top view of the one unit. (f) The single port resonator model in the coupled mode theory.

it a critical supplement between graphene with a zero or near-zero band gap and transition metal dichalcogenides (TMDs) with a wide band gap.[19−25] In addition, the band gap of BP can be flexibly tailored through electrostatic gating and surface charge transfer methods via electron/hole doping, providing additional degrees of freedom for designing tunable devices.[26,27] Therefore, as a prospective 2D material, BP can be regarded as a suitable candidate for electronic and photonic applications, such as field-effect transistors,[28] photovoltaic devices,[29] photodetectors,[30] spectral imaging,[31] ultrasensitive biosensing,[32] and so on. Increasing the interaction between light and matter is the most fundamental problem faced in the aforementioned applications, and many BP-based metamaterial structures and systems have been extensively studied to enhance light absorption or even obtain perfect absorption in monolayer or few-layer BP. However, due to the in-plane anisotropic photonic and electrical properties of 2D BP caused by its wrinkled structure with a hexagonal lattice in the phosphorus atom, most proposed schemes and designed absorption structures based on BP exhibit an anisotropic absorption response.[33−35] Although these anisotropic BP-based absorbers have the disadvantage of polarization dependence in some applications, they open the door for further research on isotropic absorbers based on anisotropic 2D materials. In 2017, Wang et al. for the first time reported a polarization-independent absorber with dual bands based on Fabry−Perot resonators. The resonators are composed of a bottom gold mirror and multiple layers of the BP metamaterial based on nanoribbon pairs, each pair of which is formed by two orthogonally stacked nanoribbons.[36] In 2020, Xia et al. studied the possibility of achieving polarization-independent optical absorption in vertically stacked anisotropic 2D BP nanostructures based on plasmon response.[37] The above schemes utilize stacked multilayer BP structures for polarization-independent absorption. Also noteworthily, in order to increase the interaction between light and atomic-scale BP in the absence of plasmon response, a large number of systems based on critical coupling with guided resonances in PC structures have been proposed in the past few years, in which just monolayer BP serves as a lossy material to attenuate the infrared and terahertz waves.[38−42] Due to the anisotropic monolayer BP deposited on the PC structures breaking the rotational symmetry of the absorption structure, these systems still exhibit polarization-dependent absorption response and hinder their further development in polarization-independent applications.

In this paper, we propose the design of a hybrid metasurface with 4-fold rotational symmetry. The hybrid metasurface consists of a patterned BP monolayer as a lossy material deposited on a lossless PC slab with a back reflector. The field distributions on the PC slab surface where the BP monolayer is deposited are greatly enhanced for a guided resonance mode, thus enhancing the light absorption capability of the BP monolayer. Under the condition that the leakage rate of the resonance mode out of the PC slab is equal to the absorption rate of the BP monolayer, critical coupling occurs, and all of the incident light at the resonant frequency is absorbed by the atomically thin 2D material, i.e., perfect absorption. Meanwhile, the absorption spectrum remains unchanged as the polarization angle of the incident light varies due to the 4-fold rotational symmetry of the system, and numerical simulation results confirm this fact. Moreover, in order to acquire a better understanding of this behavior, the mechanisms of polarization-independent absorption are further illustrated by analyzing the field distributions on the slab surface induced by two different incident waves with orthogonal polarization directions. Our work provides a simple design strategy for fabricating polarization-independent compound absorbers based on anisotropic 2D materials at frequency bands without plasmonic response.

2. STRUCTURE AND THEORETICAL MODEL

Figure 1a is a schematic diagram of monolayer BP. In order to clearly demonstrate the structure of the 2D material, two different colors are used to represent the phosphorus atoms in the upper and lower positions and the chemical bonds connecting them. The top view of monolayer BP is shown in Figure 1b. Different from graphene and TMDs with in-plane isotropy, BP exhibits a unique puckered layered structure with a hexagonal lattice in the phosphorus atom, in which there are two inequivalent geometrical directions: the armchair (AC) direction is perpendicular to the atomic ridges and the zigzag (ZZ) direction is parallel to the atomic ridges, resulting in

https://doi.org/10.1021/acsomega.4c05203
ACS Omega 2024, 9, 35052−35059

optical and electrical anisotropy in the 2D plane. The thickness of monolayer BP is much smaller than the infrared wavelength, and its photonic properties can properly be depicted by the in-plane anisotropic surface conductivities, which can be calculated by the semiclassical Drude model as follows:[33]

$$\sigma_{jj} = \frac{iD_j}{\pi\left(\omega + \frac{i\eta}{\hbar}\right)}, D_j = \frac{\pi e^2 n_S}{m_j} \quad (1)$$

where i denotes the imaginary unit, j denotes the AC or ZZ direction of BP, D_j is the Drude weight, ω is the angular frequency of the incident light, $\hbar$ is the reduced Planck constant, η is the relaxation rate, n_S is the carrier density, e represents the elementary charge, and m_j is the electron effective mass. The in-plane electron effective masses along the AC and ZZ directions can be described as

$$m_{AC} = \frac{\hbar^2}{\frac{2\gamma^2}{\Delta} + \eta_c}, m_{ZZ} = \frac{\hbar^2}{2\nu_c} \quad (2)$$

Equations 1 and 2 indicate that electrons have different effective masses in the two different directions, resulting in the anisotropic surface conductivity of BP. For monolayer BP, $\gamma = 4\alpha/\pi$eVm, $\alpha = 0.223$ nm, $\Delta = 2$ eV, $\eta_c = \hbar^2/0.4m_0$, $\nu_c = \hbar^2/1.4m_0$, and $m_0 = 9.10938 \times 10^{-31}$ kg. We chose electron doping concentration $n_S = 3 \times 10^{13}$ cm^{-2} and the relaxation rate $\eta = 10$ meV for the Drude model at room temperature. The electromagnetic field with electric field components parallel to the BP surface is capable of interacting with this 2D material and dissipating to optical loss. Figure 1c is a schematic diagram of the PC slab stacked on a metal reflector layer, consisting of a silicon slab with a square lattice of air circular holes penetrating through the PC slab. The lattice periods of the silicon PC slab in both the x and y directions are P_x and P_y, respectively. The thickness of the silicon PC slab in the z direction is h, and the radius of the air hole is R. For the convenience of discussion, the Cartesian coordinate system is marked on the PC slab in Figure 1c, and the right-handed system is used by default. Of particular interest here is the existence of guided resonance in the PC slab that can couple with the external environment.[43] Similar to the guided mode, a guided resonance also has its electromagnetic field strongly confined within the structure. Therefore, the peak field magnitude inside the slab and its surface is greatly enhanced compared to the incident wave amplitude. The light−BP interaction will be greatly enhanced in the vicinity of the frequency of the guided resonance due to the significant enhancement of the field inside the BP film covering the PC slab, which will greatly improve the absorption of BP. The BP coated on the PC slab has different physical properties along two orthogonal directions, which breaks the 4-fold rotational symmetry of the PC structure, resulting in polarization-dependent absorption characteristics of the absorber. In order to obtain a polarization-independent absorption response, a hybrid metasurface with 4-fold rotational symmetry composed of patterned BP deposited on a lossless PC slab with a back reflector is designed. Figure 1d shows the global diagram of the unit cell of the compound absorber. The top view of the unit cell is shown in Figure 1e, which clearly shows that the metasurface unit is divided into four equally sized regions. The AC and ZZ directions of the BP sheets in the upper left and lower right corners aligned along the x-axis and y-axis directions, respectively. Differently, the AC and ZZ directions of the BP sheets in the remaining two regions are along the y-axis and x-axis directions, respectively. Due to its symmetry, this structure can exhibit an isotropic absorption spectral response when light is incident normally from the upper surface of the structure. Due to the suppression of transmission by the metal back reflector at the bottom of the PC slab, the absorber can be regarded as a single-port resonant system, as shown in Figure 1f. According to the coupled-mode theory (CMT), when the plane wave with the frequency ω is launched normally into this port, the system can be expressed by the following equations:[44,45]

$$\frac{da}{dt} = (i\omega_0 - \delta - \gamma)a + \sqrt{2\gamma}S_+ \quad (3)$$

$$S_- = -S_+ + \sqrt{2\gamma}a \quad (4)$$

where a represents the normalized amplitude of the guided resonance, S_+ and S_- depict the amplitude of the normalized input and output waves, respectively, ω_0 is the resonance frequency, γ denotes the external leakage rate of the system, and δ denotes the intrinsic loss rate of the system introduced by the lossy BP monolayer. We assume that the losses of the silicon PC slab and back metal mirror are negligible. The lossless PC slab underneath supports guided resonance with electromagnetic energy strongly confined within the slab, acting as the leaky resonator. The reflection coefficient of the coupled system can be derived as

$$r = \frac{S_-}{S_+} = \frac{i(\omega - \omega_0) + \delta - \gamma}{i(\omega - \omega_0) + \delta + \gamma} \quad (5)$$

and the absorption coefficient can be described as

$$A = 1 - |r|^2 = \frac{4\delta\gamma}{(\omega - \omega_0)^2 + (\delta + \gamma)^2} \quad (6)$$

From the theoretical expressions, the light absorption performance of the system is determined by the radiation loss, the dissipative loss, and the frequency of the incident wave. As can be seen from eqs 5 and 6, when the system is driven on resonance ($\omega = \omega_0$), and the external leakage and intrinsic loss rates are the same ($\delta = \gamma$), then the critical coupling is satisfied, the reflection coefficient completely vanishes, resulting in the complete absorption of incident power, and perfect absorption can be achieved.

In order to confirm the polarization-independent perfect absorption, numerical simulations are conducted using the first-principles finite-difference time-domain (FDTD) method. In the simulations, periodic boundary conditions are applied in the x and y directions and perfectly matched layer absorption boundary conditions are used in the z direction. The plane waves are incident along the negative z-axis direction and irradiate the metamaterial absorber normally. In the numerical simulations, the patterned BP monolayer is a 2D conductive surface described by the parameters of conductivity, rather than an extremely thin medium bulk, to save computation time. A nonuniform mesh was used in the z direction, with a minimum grid size of 0.5 μm around the BP monolayer, gradually increasing away from the BP monolayer to balance computation time and memory. In the simulation calculations, the optimized structural parameters of $P_x = P_y = 30$ μm, $h = 13$ μm, and $R = 7.23$ μm are chosen. These geometric parameters remain unchanged unless otherwise specified in the following discussion. For material modeling, the refractive index of the PC slab is assumed to be 3.42, electron doping $n_S = 3 \times 10^{13}$

https://doi.org/10.1021/acsomega.4c05203
ACS Omega 2024, 9, 35052−35059

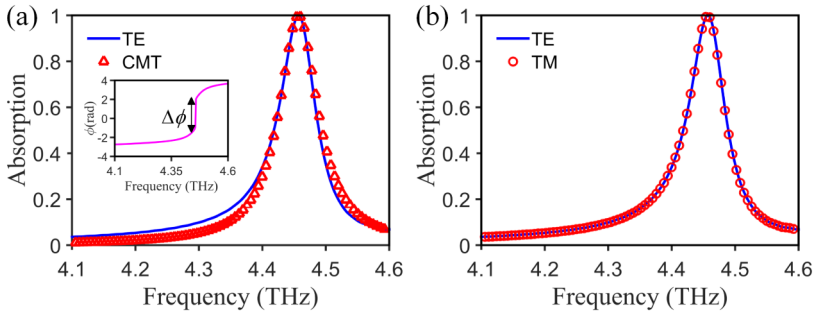

Figure 2. (a) Numerical and CMT calculated absorption spectrum of the hybrid metasurface for the TE-polarized incident wave. The excellent fit in the vicinity of the resonance validates that the system can be modeled as a single port resonator described by CMT. (b) Comparison of absorption spectra excited by TE and TM incident waves. The inset in (a) shows the reflection phase of the absorber.

cm^{-2} is adopted, and the metal reflector layer is modeled as a perfect electric conductor for simplicity. Since the metal reflector layer can block the transmission, the absorption of the designed structure equals the energy of the incident wave minus the energy of the reflected wave.

3. RESULTS AND ANALYSIS

Figure 2 exhibits the absorption spectra of the proposed structure under normal illumination. The blue solid lines in Figure 2 represent the numerical absorption spectra of the incident waves with transverse-electric (TE) polarization (i.e., incident waves with an electric field parallel to the y-axis direction). Absorption spectra of the TE-polarized incident wave show a peak absorption rate close to 1 at 4.46 THz and the Full Width at Half-Maximum (FWHM) is only Δf = 0.0711 THz, indicating that the line width of spectral absorption is very narrow. The total quality factor can be expressed as $Q = f_0/\Delta f$, which reaches about 62.7. Meanwhile, the fitted absorption curve marked by the red triangles from the CMT gives a comparison with the numerical absorption spectrum as depicted in Figure 2a, illustrating that the CMT models the system very well in the vicinity of the resonant frequency. The tiny deviation between the theory and the simulation occurs only in the regions away from resonance, as the CMT assumes that there is no loss away from the resonance. According to the CMT, the fitted intrinsic loss and external leakage of the structure are $\delta = \gamma = 0.1167$ THz. Then, the theoretical quality factor Q_{CMT} is 60 calculated by $Q_{CMT} = Q_\delta Q_\gamma/(Q_\delta + Q_\gamma)$, where the intrinsic loss is defined as $Q_\delta = \omega_0/2\delta$ and the external leakage is defined as $Q_\gamma = \omega_0/2\gamma$. The negligible difference in the quality factor between theoretical calculations and numerical simulations indicates that the perfect absorption of the absorber can be attributed to critical coupling. Another obvious piece of evidence is that when the critical coupling occurs, the resonant mode undergoes an abrupt π-phase jump across the resonant frequency, as shown in the inset of Figure 2a.[46] Next, we examined the absorption of transverse-magnetic (TM) incident waves with the electric field parallel to the x-axis direction, represented by red hollow circles in Figure 2b. As shown in Figure 2b, there is no difference in the absorption spectra between the TE and TM incident waves. The consistency of absorption along two orthogonal basis vector directions implies the achievement of polarization-independent performance.

To confirm the polarization-independent optical properties, the absorption behavior of BP-based devices is examined by changing the polarization angle of the incident light from 0° to 90°, as shown in Figure 3. The red and green arrows in Figure 3a represent the directions of the electric field and magnetic

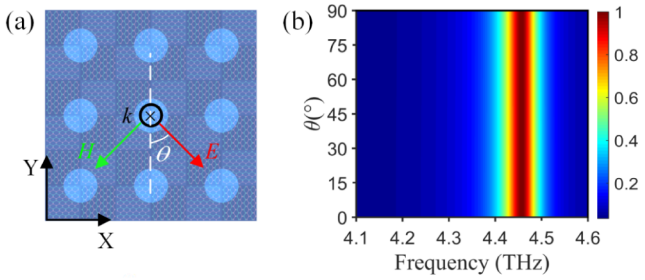

Figure 3. (a) Schematic diagram of normal irradiation on the metasurface. (b) Absorption spectra for different polarization angles. The geometric parameters of the structure are fixed to the default values.

field of the incident light, respectively. The wave vector k is perpendicular to the $x-y$ plane and points in the negative direction of the z-axis. The polarization angle θ refers to the angle between the electric field and the y-axis. The absorption spectra remain unchanged as the polarization angle increases from 0° to 90°, as shown in Figure 3b, indicating that polarization-independent absorption performance is achieved through the use of the special design. This isotropic absorption is due to the presence of the 4-fold rotational symmetry about the z-axis, not only in the geometric structure of the substrate but also in the atomic arrangement in the BP-based metasurface.

To further elucidate the underlying physics behind the isotropic absorption of the proposed structure, we examined the distributions of the magnetic field near the surface of the PC slab (where the patterned BP monolayer sits) at the peak wavelength. The first and second rows in Figure 4 represent the distributions of the magnetic field on the PC surface excited by TE and TM incident waves at the resonance frequency, respectively. First, comparing Figure 4a,e, it is evident that the field distributions of $|H_x|$ excited by the TE wave are consistent with those of $|H_y|$ excited by the TM wave after rotating 90°. Second, from Figure 4b,d, it is also clear that the TE wave-excited field distributions $|H_y|$ are the same as the TM wave-excited field distributions $|H_x|$ after rotating 90°. Lastly, Figure 4c,f show that the field distributions $|H_z|$ excited by TE and TM waves also follow the same relationship mentioned above. As is well-known, the electric field E and magnetic field H are connected by two curl equations in Maxwell's equations; thus, the in-plane components of the

https://doi.org/10.1021/acsomega.4c05203
ACS Omega 2024, 9, 35052−35059

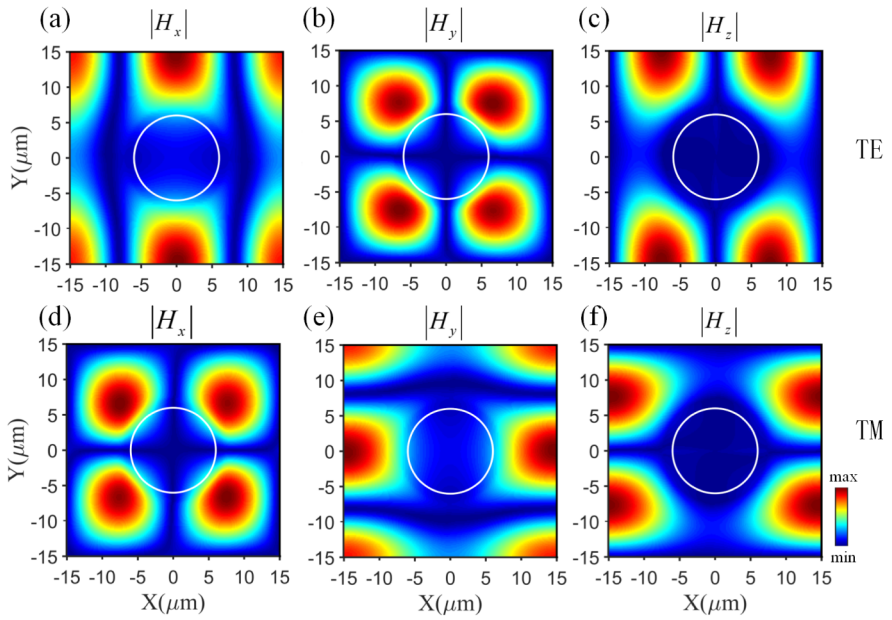

Figure 4. (a−c) Simulated magnetic field distributions on the surface of the PC slab excited by a TE incident wave at the resonant frequency. (d−f) Simulated magnetic field distributions on the surface of the PC slab excited by a TM incident wave at the resonant frequency. The boundaries of the air cylindrical holes are indicated by white circles.

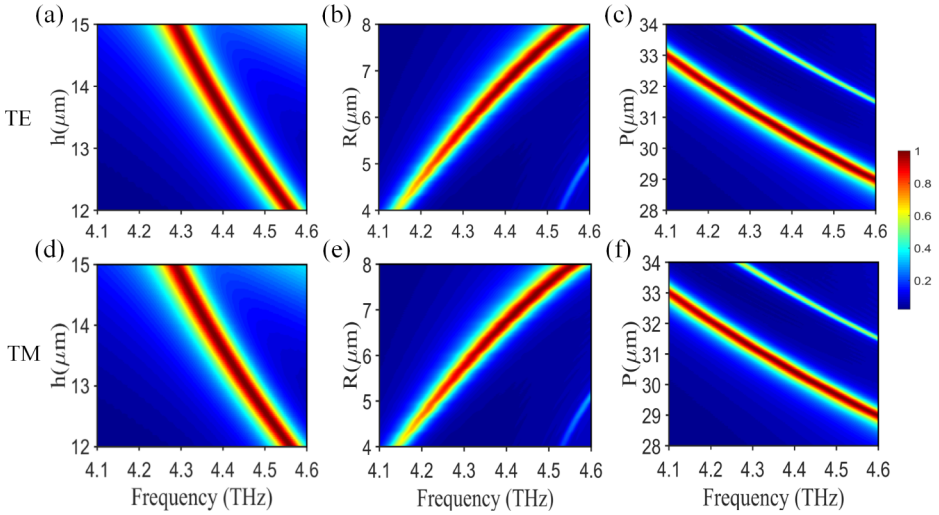

Figure 5. Simulated absorption spectra for the proposed absorber at different structural parameters under vertical illumination with TE and TM polarization, respectively. (a,d) Absorption spectra as a function of frequency and the thickness of the PC slab under vertical illumination with TE and TM polarization, respectively. (b,e) Absorption spectra as a function of frequency and air hole radius under vertical illumination with TE and TM polarization, respectively. (c,f) Absorption spectra as a function of frequency and lattice period under vertical illumination with TE and TM polarization, respectively. Except as indicated, the geometric parameters of the structure are fixed to the default values.

electric field E excited by TE waves and TM waves also follow the rotationally symmetric relationship mentioned above. The symmetries of the hybrid metasurface lead to symmetrical field distributions induced by TE and TM polarizations. Therefore, the symmetric absorption structure exhibits the same spectral response for both TE and TM incident waves, ultimately leading to polarization-independent absorption.

We have also performed additional simulations for different structural parameters to demonstrate the performance of the absorption system when deviating from the critical coupling conditions. The absorption spectra of the system with different geometric parameters under vertical illumination with TE and TM polarizations are plotted in Figure 5. The first and second rows in Figure 5 correspond to the absorption spectra of the TE and TM incident waves, respectively. It is evident that the absorption spectra of TE and TM waves are the same, indicating that if the changes in geometric parameters do not affect the symmetry, the isotropic absorption characteristics will not be altered. Figure 5a,d show the absorption spectra as functions of frequency and the thickness of the PC slab. The external leakage rate γ of the resonance is relatively stable with respect to h, and the absorption of 2D BP is approximately independent of the resonance frequency in this regime. Since the placement of the guided resonance frequency is not crucial, controlling the external leakage rate plays a dominant role in achieving the critical coupling. These factors together contribute to the maintenance of critical coupling in spite of a significant change of the resonant frequencies. Therefore, the

https://doi.org/10.1021/acsomega.4c05203
ACS Omega 2024, 9, 35052−35059

high absorption remains largely unchanged when the thickness h is increased from 12 to 15 μm. The spectral position of the absorption peak tends to exhibit a red shift with the thickness increase, as the effective refractive index of the guided resonance increases with an increasing thickness of the PC slab. Figure 5b,e show the absorption spectra as a function of the frequency and the air hole radius. According to eq 6, the bandwidth of the absorption spectrum is determined by the sum of the external leakage rate and loss rate, i.e., $(\gamma + \delta)/\pi$. For the PC slab, the external leakage rate of the guided resonance depends mostly on the ratio of the hole radius to the period, namely, the R/P. Specifically, the external leakage rate γ increases as the radius of the hole increases when the period is fixed. In addition, the resonance intrinsic loss rate δ resulting from the BP monolayer is considered to be largely radius-independent. Thus, the FWHM of the absorption spectrum of guided resonance increases as the hole radius increases, as shown in Figure 5b,e. In these ranges of radius, the system evolves from under coupling($\delta > \gamma$), through critical coupling, to the over coupling($\delta < \gamma$) regime when gradually increasing the radius. The absorption performance of the metasurface can also be tuned by filling the air holes with different dielectric materials. The related rules are the same as discussed in ref 38 but unlike the absorber in the literature, this proposed system has isotropic absorption response. In addition to the geometric parameters of the structure, the doping concentration of BP is also an important variable that can affect the absorption performance of the absorber. According to eq 1, surface conductivities depend on the doping concentration, so the doping concentration can regulate the intrinsic loss rate δ. Therefore, the absorption bandwidth $(\gamma + \delta)/\pi$ can be regulated by changing the doping concentration. Figure 6

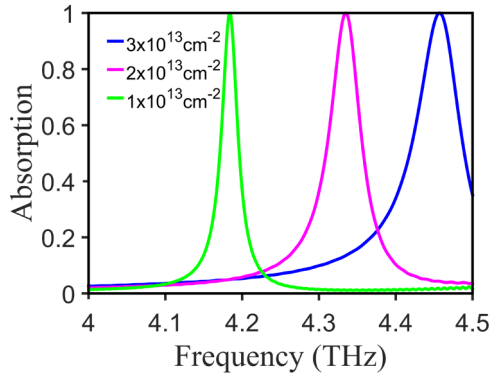

Figure 6. (a) Numerical absorption spectra of the proposed structure at different doping concentrations. The blue curve represents the absorption spectrum at a doping concentration of 3×10^{13} cm^{-2} and an air hole radius of 7.23 μm. The magenta curve represents the absorption spectrum at a doping concentration of 2×10^{13} cm^{-2} and an air hole radius of 6.2 μm. The green curve represents the absorption spectrum at a doping concentration of 1×10^{13} cm^{-2} and an air hole radius of 4.7 μm. Except for the radius of the hole, the geometric parameters of the PC slab are fixed to default values.

shows absorption spectra of the proposed structure at doping concentrations $n_S = 3 \times 10^{13}$ cm^{-2}, $n_S = 2 \times 10^{13}$ cm^{-2}, and $n_S = 1 \times 10^{13}$ cm^{-2}, where the absorption states are in critical coupling. When changing the doping concentration, the absorption state remains critical coupling, as the radius of the air hole is adjusted appropriately to ensure that the leakage rate remains equal to the intrinsic loss. As the doping concentration decreases, the radius used gradually decreases, with radii of 7.23 μm, 6.2 μm, and 4.7 μm, respectively. As shown in Figure 6, in addition to the red shift of the resonance peak, the absorption bandwidth significantly shrinks as a result of the simultaneous decrease of the doping concentration and leakage rate. This method demonstrates the manipulation of the absorption bandwidth while maintaining the theoretical maximum absorptivity, which suggests advantages in efficiency and flexibility of BP-based absorbers, detectors, modulators, filters, and so on. Some previous reports have also revealed such possibility of absorption bandwidth manipulation in a graphene system by simultaneously changing the asymmetric parameter of metasurfaces, the Fermi level, and the layer number of graphene.[47] Changing the doping concentration will not break the symmetry of the hybrid BP metasurface, and the absorption spectrum will still maintain isotropy. The approach of using the 4-fold rotational symmetry (i.e., C_4 symmetry) in a unit cell to construct a polarization-independent metasurface, including utilizing quasi-bound states in the continuum to achieve perfect absorbers and high-order harmonic generation, has been mentioned in some previous works.[48,49]

4. CONCLUSIONS

In conclusion, the present work theoretically proposed and investigated a BP-based absorber operating at terahertz frequencies that shows polarization-independent responses, through the use of a 4-fold rotational symmetric structure that consists of a lossy patterned BP monolayer, a PC slab, and a back reflection mirror. Furthermore, the absorption of the BP monolayer can reach 100% by utilizing PC-guided resonance to achieve a critical coupling to the BP monolayer. The results open up possibilities of devising BP-based photodetectors and sensors with isotropic absorption characteristics. Moreover, the simple design concept could be extended to other anisotropic 2D materials such as borophene.

AUTHOR INFORMATION

Corresponding Author

Xuewen Long − *Institute of Medical Physics, Hunan University of Medicine, Huaihua 418000, China;* orcid.org/0000-0002-3688-6048; Email: xwlong77@126.com

Authors

Jing Bai − *Department of Physics, Taiyuan Normal University, Jinzhong 030619, China;* orcid.org/0000-0002-5800-2856

Yingjun Zhang − *Institute of Medical Physics, Hunan University of Medicine, Huaihua 418000, China*

Mingshan Zhu − *Institute of Medical Physics, Hunan University of Medicine, Huaihua 418000, China*

Xiuli Guo − *Institute of Medical Physics, Hunan University of Medicine, Huaihua 418000, China*

Jin Wang − *Department of Physics, Taiyuan Normal University, Jinzhong 030619, China*

Weiqiang Wang − *School of Electronic Information and Artificial Intelligence, Shaanxi University of Science and Technology, Xi' an 710021, China*

Rui Lou − *Center for Attosecond Science and Technology, Xi'an Institute of Optics and Precision Mechanics, Chinese Academy of Sciences, Xi'an 710119, China*

Complete contact information is available at: https://pubs.acs.org/10.1021/acsomega.4c05203

https://doi.org/10.1021/acsomega.4c05203
ACS Omega 2024, 9, 35052−35059

Notes

The authors declare no competing financial interest.

■ ACKNOWLEDGMENTS

The authors acknowledge the National Natural Science Foundation of China (62075238), the Hunan Provincial Natural Science Foundation of China (2024JJ7326), the Scientific Research Foundation of Hunan University of Medicine in China (2020122002), and the Scientific and Technological Innovation Programs of Higher Education Institutions in Shanxi (2021L421).

■ REFERENCES

(1) Novoselov, K. S.; Jiang, D.; Schedin, F.; Booth, T. J.; Khotkevich, V. V.; Morozov, S. V.; Geim, A. K. Two-dimensional atomic crystals. *Proc. Natl. Acad. Sci. U. S. A.* **2005**, *102* (30), 10451−10451.
(2) Vakil, A.; Engheta, N. Transformation optics using graphene. *Science* **2011**, *332* (6035), 1291−1291.
(3) Lu, H.; Gan, X.; Mao, D.; Fan, Y.; Yang, D.; Zhao, J. Nearly perfect absorption of light in monolayer molybdenum disulfide supported by multilayer structures. *Opt. Express* **2017**, *25* (18), 21630−21630.
(4) Fang, Z.; Thongrattanasiri, S.; Schlather, A.; Liu, Z.; Ma, L.; Wang, Y.; Ajayan, P. M.; Nordlander, P.; Halas, N. J.; García de Abajo, F. J. Gated tunability and hybridization of localized plasmons in nanostructured graphene. *ACS Nano* **2013**, *7* (3), 2388−2388.
(5) Wang, W.; Klots, A.; Yang, Y.; Li, W.; Kravchenko, I. I.; Briggs, D. P.; Bolotin, K. I.; Valentine, J. Enhanced absorption in two-dimensional materials via Fano-resonant photonic crystals. *Appl. Phys. Lett.* **2015**, *106* (18), 181104.
(6) Li, H.; Ren, Y.; Hu, J.; Qin, M.; Wang, L. Wavelength-selective wide-angle light absorption enhancement in monolayers of transition-metal dichalcogenides. *J. Light. Technol.* **2018**, *36* (16), 3236−3236.
(7) Jiang, Y.; Chen, W.; Wang, J. Broadband MoS_2-based absorber investigated by a generalized interference theory. *Opt. Express* **2018**, *26* (19), 24403−24403.
(8) Jiang, Y.; Zhang, H. D.; Wang, J.; Gao, C. N.; Wang, J.; Cao, W. P. Design and performance of a terahertz absorber based on patterned graphene. *Opt. Lett.* **2018**, *43* (17), 4296−4296.
(9) Shiue, R.-J.; Gan, X.; Gao, Y.; Li, L.; Yao, X.; Szep, A.; Walker, D., Jr; Hone, J.; Englund, D. Enhanced photodetection in graphene-integrated photonic crystal cavity. *Appl. Phys. Lett.* **2013**, *103* (24), 241109.
(10) Xiang, Y.; Dai, X.; Guo, J.; Zhang, H.; Wen, S.; Tang, D. Critical coupling with graphene-based hyperbolic metamaterials. *Sci. Rep.* **2014**, *4* (1), 5483.
(11) Piper, J. R.; Fan, S. Total absorption in a graphene monolayer in the optical regime by critical coupling with a photonic crystal guided resonance. *ACS Photon.* **2014**, *1* (4), 347−347.
(12) Liu, Y.; Chadha, A.; Zhao, D.; Piper, J. R.; Jia, Y.; Shuai, Y.; Menon, L.; Yang, H.; Ma, Z.; Fan, S.; Xia, F.; Zhou, W. Approaching total absorption at near infrared in a large area monolayer graphene by critical coupling. *Appl. Phys. Lett.* **2014**, *105* (18), 181105.
(13) Li, H.; Qin, M.; Wang, L.; Zhai, X.; Ren, R.; Hu, J. Total absorption of light in monolayer transition-metal dichalcogenides by critical coupling. *Opt. Express* **2017**, *25* (25), 31612−31612.
(14) Wu, J.; Wang, H.; Jiang, L.; Guo, J.; Dai, X.; Xiang, Y.; Wen, S. Critical coupling using the hexagonal boron nitride crystals in the mid-infrared range. *J. Appl. Phys.* **2016**, *119* (20), 203107.
(15) Jiang, X.; Wang, T.; Xiao, S.; Yan, X.; Cheng, L. Tunable ultra-high-efficiency light absorption of monolayer graphene using critical coupling with guided resonance. *Opt. Express* **2017**, *25* (22), 27028−27028.
(16) Xiao, S.; Liu, T.; Wang, X.; Liu, X.; Zhou, C. Tailoring the absorption bandwidth of graphene at critical coupling. *Phys. Rev. B* **2020**, *102* (8), 085410.
(17) Wang, J.; Yang, J.; Shi, D. Perfect absorption for monolayer transition-metal dichalcogenides by critical coupling. *Nanotechnology* **2020**, *31* (46), 465205.
(18) Liu, T.; Zhou, C.; Xiao, S. Tailoring anisotropic absorption in a borophene-based structure via critical coupling. *Opt. Express* **2021**, *29* (46), 8941−8941.
(19) Li, L.; Yu, Y.; Ye, G. J.; Ge, Q.; Ou, X.; Wu, H.; Feng, D.; Chen, X. H.; Zhang, Y. Black phosphorus field-effect transistors. *Nat. Nanotechnol.* **2014**, *9* (5), 372−372.
(20) Xu, Y.; Wang, Z.; Guo, Z.; Huang, H.; Xiao, Q.; Zhang, H.; Yu, X. Solvothermal synthesis and ultrafast photonics of black phosphorus quantum dots. *Adv. Opt. Mater.* **2016**, *4* (8), 1223−1223.
(21) Liang, L.; Wang, J.; Lin, W.; Sumpter, B. G.; Meunier, V.; Pan, M. Electronic bandgap and edge reconstruction in phosphorene materials. *Nano Lett.* **2014**, *14* (11), 6400−6400.
(22) Koenig, S. P.; Doganov, R. A.; Schmidt, H.; Castro Neto, A. H.; Özyilmaz, B. Electric field effect in ultrathin black phosphorus. *Appl. Phys. Lett.* **2014**, *104* (10), 103106.
(23) Xia, F.; Wang, H.; Jia, Y. Rediscovering black phosphorus as an anisotropic layered material for optoelectronics and electronics. *Nat. Commun.* **2014**, *5*, 4458.
(24) Tran, V.; Soklaski, R.; Liang, Y.; Yang, L. Layer-controlled band gap and anisotropic excitons in few-layer black phosphorus. *Phys. Rev. B* **2014**, *89*, 235319.
(25) Zhang, R.; Zhang, Y.; Yu, H.; Zhang, H.; Yang, R.; Yang, B.; Liu, Z.; Wang, J. Broadband black phosphorus optical modulator in the spectral range from visible to mid-infrared. *Adv. Opt. Mater.* **2015**, *3*, 1787−1792.
(26) Koenig, S. P.; Doganov, R. A.; Seixas, L.; Carvalho, A.; Tan, J. Y.; Watanabe, K.; Taniguchi, T.; Yakovlev, N.; Castro Neto, A. H.; Özyilmaz, B. Electron Doping of Ultrathin Black Phosphorus with Cu Adatoms. *Nano Lett.* **2016**, *16* (4), 2145−2145.
(27) Deng, B.; Tran, V.; Xie, Y.; Jiang, H.; Li, C.; Guo, Q.; Wang, X.; Tian, H.; Koester, S. J.; Wang, H.; et al. Efficient electrical control of thin-film black phosphorus bandgap. *Nat. Commun.* **2017**, *8* (1), 14474.
(28) Dickerson, W.; Tayari, V.; Fakih, I.; Korinek, A.; Caporali, M.; Serrano-Ruiz, M.; Peruzzini, M.; Heun, S.; Botton, G. A.; Szkopek, T. Phosphorus oxide gate dielectric for black phosphorus field effect transistors. *Appl. Phys. Lett.* **2018**, *112* (17), 173101.
(29) Shang, A.; Li, X. Photovoltaic devices: Opto-electro-thermal physics and modeling. *Adv. Mater.* **2017**, *29* (8), 1603492.
(30) Venuthurumilli, P. K.; Ye, P. D.; Xu, X. Plasmonic resonance enhanced polarization-sensitive photodetection by black phosphorus in near infrared. *ACS Nano* **2018**, *12* (5), 4861−4861.
(31) Engel, M.; Steiner, M.; Avouris, P. Black phosphorus photodetector for multispectral, high-resolution imaging. *Nano Lett.* **2014**, *14* (11), 6414−6414.
(32) Yuan, Y.; Yu, X.; Ouyang, Q.; Shao, Y.; Song, J.; Qu, J.; Yong, K. T. Highly anisotropic black phosphorous-graphene hybrid architecture for ultrassensitive plasmonic biosensing: Theoretical insight. *2D Mater.* **2018**, *5* (2), 025015.
(33) Liu, Z.; Aydin, K. Localized surface plasmons in nanostructured monolayer black phosphorus. *Nano Lett.* **2016**, *16* (6), 3457−3457.
(34) Feng, N.; Zhu, J.; Li, C.; Zhang, Y.; Wang, Z.; Liang, Z.; Liu, Q. H. Near-unity anisotropic infrared absorption in monolayer black phosphorus with/without subwavelength patterning design. *IEEE J. Sel. Top. Quantum Electron.* **2019**, *25* (3), 1−1.
(35) Ni, X.; Wang, L.; Zhu, J.; Chen, X.; Lu, W. Surface plasmons in a nanostructured black phosphorus flake. *Opt. Lett.* **2017**, *42* (13), 2659−2659.
(36) Wang, J.; Jiang, Y.; Hu, Z. Dual-band and polarization-independent infrared absorber based on two-dimensional black phosphorus metamaterials. *Opt. Express* **2017**, *25* (18), 22149−22149.
(37) Xia, S. X.; Zhai, X.; Wang, L. L.; Wen, S. C. Polarization-independent plasmonic absorption in stacked anisotropic 2D material nanostructures. *Opt. Lett.* **2020**, *45* (1), 93−93.

https://doi.org/10.1021/acsomega.4c05203
ACS Omega 2024, 9, 35052−35059

(38) Qing, Y. M.; Ma, H. F.; Cui, T. J. Tailoring anisotropic perfect absorption in monolayer black phosphorus by critical coupling at terahertz frequencies. *Opt. Express* **2018**, *26*, 32442−32450.
(39) Liu, T.; Jiang, X.; Zhou, C.; Xiao, S. Black phosphorus-based anisotropic absorption structure in the mid-infrared. *Opt. Express* **2019**, *27* (20), 27618−27618.
(40) Xu, Y.; Li, H.; Zhang, X.; Bai, Z.; Zhang, Z.; Qin, S. Triple-band black-phosphorus-based absorption using critical coupling. *Appl. Opt.* **2020**, *59* (28), 9003−9003.
(41) Liu, T.; Jiang, X.; Wang, H.; Liu, Y.; Zhou, C.; Xiao, S. Tunable anisotropic absorption in monolayer black phosphorus using critical coupling. *Appl. Phys. Express* **2020**, *13* (1), 012010.
(42) Yuan, Z.; Liu, Y.; Zong, X.; Chen, Z.; Liu, Y. Anisotropic perfect absorber at mid-infrared wavelengths using black phosphorus-based metasurfaces. *Opt. Laser Technol.* **2024**, *175*, 110778.
(43) Fan, S.; Joannopoulos, J. D. Analysis of guided resonances in photonic crystal slabs. *Phys. Rev. B* **2002**, *65* (23), 235112.
(44) Haus, H. A. *Waves and Fields in Optoelectronics*; Prentice−Hall: Engle−wood Cliffs, NJ, 1984.
(45) Haus, H. A.; Huang, W. Coupled-mode theory. *Proc. IEEE* **1991**, *79* (10), 1505−1505.
(46) Yoon, J.; Seol, K. H.; Song, S. H.; Magnusson, R. Critical coupling in dissipative surface-plasmon resonators with multiple ports. *Opt. Express* **2010**, *18* (25), 25702−25711.
(47) Wang, X.; Duan, J.; Chen, W.; Zhou, C.; Liu, T.; Xiao, S. Controlling light absorption of graphene at critical coupling through magnetic dipole quasi-bound states in the continuum resonance. *Phys. Rev. B* **2020**, *102*, 155432.
(48) Saadabad, R. M.; Huang, L.; Miroshnichenko, A. E. Polarization-independent perfect absorber enabled by quasibound states in the continuum. *Phys. Rev. B* **2021**, *104*, 235405.
(49) Xiao, S.; Qin, M.; Duan, J.; Liu, T. Robust enhancement of high-harmonic generation from all-dielectric metasurfaces enabled by polarization-insensitive bound states in the continuum. *Opt. Express* **2022**, *30* (18), 32590−32590.

https://doi.org/10.1021/acsomega.4c05203
ACS Omega 2024, 9, 35052−35059